International Journal of Refractory Metals and Hard Materials 113 (2023) 106165

Contents lists available at ScienceDirect

International Journal of Refractory Metals and Hard Materials

journal homepage: www.elsevier.com/locate/IJRMHM

Development of TaC-based transition metal carbide superlattices via compound target magnetron sputtering

Barbara Schmid [a,*], Nikola Koutná [a], Rainer Hahn [b], Tomasz Wojcik [a], Peter Polcik [c], Paul Heinz Mayrhofer [a]

[a] Institute of Materials Science and Technology, Technische Universität Wien, Getreidemarkt 9, 1060 Wien, Austria
[b] Christian Doppler Laboratory for Surface Engineering of high-performance Components, Technische Universität Wien, Getreidemarkt 9, 1060 Wien, Austria
[c] Plansee Composite Materials GmbH, Siebenbürgerstraße 23, 86983 Lechbruck am See, Germany

ARTICLE INFO

Keywords:
Superlattice
Carbide
Transition metal
Hardness
Tantalum

ABSTRACT

Transition metal carbides belong to ultra-high temperature ceramics and are particularly valued for their high thermal and mechanical stability as well as melting points of even above 4000 °C. However, a considerable limitation of these materials is their high inherent brittleness. Inspired by the success of nanolayered superlattice architecture—shown to enhance both hardness and toughness of transition metal (TM) nitrides—we developed superlattice films with TM carbides. Among these, density functional theory calculations suggest TaC/HfC and TiC/TaC to have a similar shear modulus mismatch of 23 and 19 GPa, but a different lattice parameter mismatch of 4.2 and 2.4%, respectively. Detailed transmission electron microscopy and X-ray diffraction show a pronounced superlattice structure for TiC/TaC with nominal bilayer periods Λ_{nom} of 2, 6, and 10 nm. Contrary, the TaC/HfC showed a more solid solution like characteristic for $\Lambda_{nom} = 2$ nm, and a clear superlattice structure for $\Lambda_{nom} = 6$ and 10 nmjap. While the hardness of the TaC/HfC coatings is between those of their constituents TaC (33.3 ± 1.9 GPa) and HfC (37.4 ± 3.2 GPa), the TiC/TaC superlattices outperform their constituents and clearly show a superlattice-effect with a peak of 44.1 ± 3.4 GPa at $\Lambda_{nom} = 2$ nm (TiC has 37.6 ± 3.1 GPa). Also the qualitative fracture behavior investigation with 450-mN-loaded cube corner indentation yield the TiC/TaC superlattices to be superior to the TaC/HfC as well as the monolithically prepared TiC, TaC, and HfC coatings.

1. Introduction

Materials exhibiting excellent thermal stability, oxidation and wear resistance have been at the center of both academic as well as industrial attention for many years, especially in the realms of protecting machining tools and components used in the automotive, aerospace, and energy sectors [1,2]. Early transition metal carbides feature excellent strengths and thermal stability of up to well over 3000 °C and high hardness values, hence are often referred to as ultra-high temperature ceramics (UHTC) [3]. However, a significant downside of transition metal carbides is their high inherent brittleness [4]. Various approaches were established to increase the performance of transition metal ceramics. Among the most successful ones is the so-called superlattice architecture.

Superlattice coatings are multilayered systems that periodically alternate nanoscale layers of two or more materials. By controlling the thickness of the individual layers, many physical properties—such as optical, magnetic, or mechanical—can be affected and fine-tuned. An excellent example is the superlattice-induced hardness enhancement, first reported by Helmersson et al. for TiN/VN superlattices [5]. In this study, nanolayered films with a bilayer period of 5.2 nm exhibit an almost two times higher hardness compared to their monolithic TiN and VN constituents. Later, Chu and Barnett [6] related this effect to impeded dislocation gliding abilities across individual layers. In order to maximize the hardness enhancement effect, the materials should have different shear moduli as well as lattice parameters [7]. Thus, the line energy of dislocations should be as different as possible in the adjacent layers and coherency strain fields (due to coherently grown layers with slightly different lattice parameters) should further restrict dislocation glide across the interfaces. Therefore, the superlattice effect is often named a combination of coherency-strain hardening (as observed by Cahn for spinodal decomposition and thus refered to as Cahn model [8])

* Corresponding author.
E-mail addresses: Barbara.schmid@tuwien.ac.at (B. Schmid), Nikola.koutna@tuwien.ac.at (N. Koutná), rainer.hahn@tuwien.ac.at (R. Hahn), Tomasz.wojcik@tuwien.ac.at (T. Wojcik), Peter.polcik@plansee.com (P. Polcik), Paul.mayrhofer@tuwien.ac.at (P.H. Mayrhofer).

https://doi.org/10.1016/j.ijrmhm.2023.106165
Received 29 October 2022; Received in revised form 14 February 2023; Accepted 21 February 2023
Available online 6 March 2023

and Koehler strengthening (where dislocations are confined to within layers at interfaces; also referred to as modulus difference strengthening) [9]. Recent publications suggest that the superlattice architecture also improves fracture toughness [6,7].

In recent years, several publications—examples include TiN/CrN [10,11], TiN/WN [12], MoN/TaN [13,14], TiN/(Cr,Al)N [15], or TiN/MoN [16]—studied hardness and fracture toughness enhancement in transition metal nitride superlattices. However, this is not the case for carbide superlattices, especially for films synthesized via magnetron sputtering [17]. Our work aims to showcase that the concepts valid for nitrides extend to the even more brittle carbides. In particular, we focus on the effect of lattice mismatch and shear modulus mismatch on the hardness of carbide superlattices. Preliminary high throughput density functional theory (DFT) simulations were performed via the Vienna Ab Initio Simulation Package (VASP), using the projector augmented plane wave pseudopotentials (PAW) [16,18,19]. For the approximation of exchange-correlation effects, the general gradient approximation (GGA) was used with a Perdew-Burke-Ernzerhof functional (PBE) [12]. Of all possibilities, two material systems—TaC/HfC and TiC/TaC—were chosen on the grounds of structural stability, shear modulus mismatch, and lattice parameter mismatch [20]. Density functional theory simulations by Koutná et al. [20] show that the TaC/HfC system provides a significant shear modulus difference as well as lattice parameter mismatch. Contrary, the TiC/TaC system provides a smaller shear modulus and lattice parameter mismatch [20].

2. Materials and methods

TaC/HfC and TiC/TaC superlattices as well as the corresponding monolithically grown films were synthesized using non-reactive DC and pulsed DC unbalanced magnetron sputtering with an AJA International Orion 5 system. The TaC layers are prepared with the help of a corresponding 2″ target whereas the TiC and HfC layers are obtained from respective 3″ targets (all targets, with ≥99.5% purity and density are provided by Plansee Composite Materials GmbH [13]). The nominal bilayer period Λ_{nom}, comprising equally thick layers, was adjusted by a computer-controlled shutter system to be either 2, 6, or 10 nm across the entire film thickness of ~1 μm.

The substrates (Si(100) and austenitic stainless steel with dimensions of 7x20x0.35 mm^3 and 7x20x1 mm^3, respectively) were pre-cleaned in acetone and ethanol using an ultrasonic bath for 5 min each. The base pressure of the chamber was below 10^{-4} Pa for all depositions. Using a load lock, we placed the substrates inside the chamber, thermally cleaned them at 600 °C for 20 min, and plasma etched them at an Ar pressure of 6 Pa and a negative potential of −750 V for 10 min at the same temperature. The films were synthesized at 600 °C and 0.4 Pa Ar pressure. The targets were powered with 5.6 W/cm^2 for TiC, 7.3 W/cm^2 for HfC, and 9.3 W/cm^2 for TaC to ensure dense growth morphologies. The 3″ targets were operated in pulsed DC mode with a pulse frequency of 150 kHz and a pulse width of 2576 ns. A negative constant bias potential of −30 V was applied to the substrates.

All X-ray diffraction measurements were conducted in symmetric Bragg-Brentano mode using Cu-K_α radiation on a Panalytical XPert PRO MPD appliance. The lattice parameters were obtained from X-ray diffractograms using Eq. (1):

$$4a^2 sin^2(\theta) = \lambda^2\left(h^2 + k^2 + l^2\right), \quad (1)$$

where a refers to the lattice parameter, θ to the diffraction angle, λ to the wavelength of the Cu-K_α radiation and h, k, and l to the Miller indices of the reflex. From the diffraction patterns with satellite reflexes, the bilayer period Λ can be calculated using the following modified Bragg's law equation:

$$\frac{2sin\theta_n - 2sin\theta_{SL}}{\lambda} = \pm\frac{n}{\Lambda} \quad (2)$$

where θ_{SL} refers to the diffraction angle of the main Bragg peak, θ_n to the diffraction angle of the corresponding satellite reflexes of that peak, λ to the wavelength of the Cu-K_α radiation and n to the order of the satellite peak [21].

Transmission electron microscopy (TEM) examinations were performed with an FEI TECNAI F20 operating at an acceleration voltage of 200 kV. We used a standard lift-out method to prepare the TEM samples employing a focused ion beam (FIB) workstation (ThermoFisher Scios2).

Morphology and coating thickness of the material systems were studied by scanning electron microscopy (SEM). Cross-sectional images were taken using an FEI Quanta 250 field emission gun scanning electron microscope (FEGSEM) equipped with both a secondary electron and a back-scattered electron detector at an acceleration voltage of 5 kV.

Indentation hardness H and modulus E are derived from analysing the load-displacement curves obtained from nanoindentation measurements using a Fisher Cripps Laboratories ultra-microindentation system (UMIS) equipped with a Berkovich indenter tip following the guidelines of Refs. [22,23]. Thirty indents with loads up to 15 mN were performed for each measurement. A qualitative assessment of the fracture toughness was conducted with the same system, for which a cube corner tip was mounted [24]. The indents performed with 50 to 450 mN load were analyzed on a ZEISS Sigma 500 VP FEGSEM.

The material composition was acquired using energy dispersive X-ray spectroscopy (EDS) on an FEI Philips XL 30 SEM equipped with an EDAX Sapphire EDS system, calibrated using coatings that have been quantified with elastic recoil detection analysis (ERDA).

3. Results

3.1. Structure

Fig. 1 shows XRD patterns recorded for the monolithically grown carbides (TiC, TaC, HfC) and the superlattice films on Si (100) substrates. The peak sequences of the monolithic coatings perfectly follow the face- centred cubic (fcc) crystal structure of the NaCl prototype. The superlattice coatings show a cumulative peak between the positions of the constituting phase-pure layers—indicating their coherent growth—and up to three orders of satellite peaks around that reflex. Theses so-called superlattice reflexes arise from the constructive interference of X-ray beams reflected from the top and bottom interfaces of the TaC/HfC respectively TiC/TaC bilayer units. Thus, the more pronounced these are, the better is the long-range coherent periodicity of these bilayers and the higher is the quality of the SL in terms of flat and homogeneous interfaces. As the bilayer period increases, the satellite peaks become more prominent and move closer to the main Bragg peak. The presence of native oxide on the Silicon substrates generally yields in polycrystalline thin films [13]. The corresponding lattice parameters agree well with literature and DFT data, see Table 1 [20,25]. The reflex at ~33° 2θ stems from the Si(100) substrate and is sometimes hidden behind the (111) peak of the film. The (100) peak of hexagonal Ta_2C is also located in this exact position [25]. To ensure that this peak stems from Si and not from Ta_2C, additional XRD measurements featuring a tilted (3°) stage were performed to block out substrate reflexes, see the additional XRD pattern for TaC in Fig. 1. Clearly, this peak is not present when tilting the sample, which proves that the TaC is purely fcc structured. Additionally, the samples grown on austenite substrates miss this XRD peak at ~33°. HfC generally exhibits no preferred growth orientation, whereas TiC shows a dominating (111)-oriented and TaC more of a (200)-oriented growth. However, both superlattice systems exhibit no preferred growth orientation, although there is a slight trend towards a more (111)-oriented growth for TaC/HfC and a more (200)-oriented growth for TiC/TaC. Contrary to the TaC/HfC system, the TiC/TaC coatings show pronounced satellite reflexes, suggesting that the latter are of a higher quality (in terms of flat interfaces and long-range coherent periodicity). These satellite reflexes were used to calculate

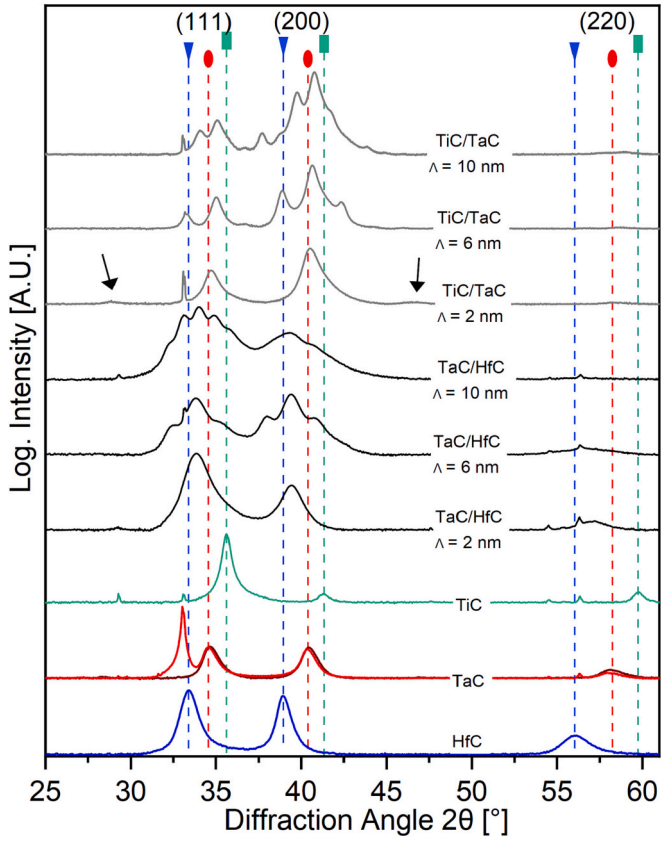

Fig. 1. X-ray diffraction patterns of monolithic thin films as well as superlattice structures. The three at the bottom refer to the monotithic carbides, the three in the middle to TaC/HfC and the top three to TiC/TaC coatings. For monolithically grown TaC, two XRD patterns are overlaid. The dark red one, which misses the peak at 2θ ~33°, was conducted with a 3°-tilted stage. This proves that this peak is not from the coating but the single-crystalline Si substrate. (For interpretation of the references to colour in this figure legend, the reader is referred to the web version of this article.)

Table 1
Nominal and experimentally obtained bilayer periods (Λ_{nom} and Λ_{exp}) for our superlattices. The TaC/HfC superlattice with Λ_{nom} = 2 nm did not show XRD satellite peaks and no individual layers during the TEM investigation (Fig. 2). The experimentally obtained lattice parameters (a_{XRD}) are opposed to literature and DFT values (a_{lit} and a_{DFT}). Additionally, the DFT values of the corresponding shear moduli G are given.

Material System	Λ_{nom} [nm]	Λ_{exp} [nm]	a_{lit} [nm]	a_{DFT} [nm]	a_{XRD} [nm]	G_{DFT} [GPa]
HfC	–		0.465 [26]	0.465 [20]	0.468	180
TaC	–		0.445 [27]	0.448 [20]	0.449	157
TiC	–		0.429 [27]	0.434 [20]	0.438	176
TaC/HfC	2	–			0.457	
	6	6.24				
	10	10.03				
TiC/TaC	2	1.66				
	6	5.71				
	10	9.76				

the experimental bilayer period (Λ_{exp}), see Table 1. No satellite peaks could be detected for the TaC/HfC coating with a nominal bilayer period of Λ_{nom} = 2 nm. Thus, for this coating no Λ_{exp} is given in Table 1. Likewise, the TiC/TaC coatings with Λ_{nom} = 2 nm exhibit no apparent superlattice reflexes, although the low-intensity features at 2θ ~27 and 47° (marked with arrows) may indicate such. Therefore, these were investigated in more detail by TEM, see the upcoming chapter.

The lattice parameters of the monolithically grown layers are close to literature and DFT data, see Table 1. Further, for the TaC/HfC coating with Λ_{nom} = 2 nm, we calculated the lattice parameter, as this coating did not show superlattice reflexes and also during TEM investigations, no individual layers were present.

3.2. Growth morphology

The cross-sectional scanning transmission electron microscopy (STEM) investigations of the TaC/HfC coating with a nominal bilayer period of 2 nm, Fig. 2a, shows no layered structure, as already suggested by the XRD investigations due to the absence of superlattice reflexes. For TaC/HfC coatings with a larger Λ_{nom}, the individual layers can clearly be identified, as shown in Fig. 2b for Λ_{nom} = 6 nm, proving its superlattice structure. The respective selected area electron diffraction (SAED) patterns (insets of Figs. 2a and b) nicely show their phase-pure face centred cubic structure (NaCl type). These SAED patterns also show the reflexes from the Si(100) substrate, which were used as a reference for indexing the ring-like pattern of TaC. All patterns from the film could thus be identified as purely fcc type, as suggested by XRD. Cross-sectional STEM investigations of the TiC/TaC coatings highlight that there is also a layered structure present (Fig. 2c) for Λ_{nom} = 2 nm. XRD investigations did not show pronounced superlattice reflexes for this superlattice structure, see Fig. 1. When comparing the TaC/HfC and TiC/TaC coatings with Λ_{nom} = 2 nm (Fig. 2c and d, respectively) the layered arrangement is easier to identify for the TiC/TaC coatings, due to the significant Z-contrast between TiC and TaC, which is not that pronounced between TaC and HfC. Like the TaC/HfC coatings, the TiC/TaC coatings solely show a face cantered cubic ring-like pattern during the SAED investigations, insets of Fig. 2.

3.3. Chemical composition

EDS investigations suggest that all coatings—the monolithically grown TiC, TaC, and HfC, as well as the TaC/HfC and TiC/TaC coatings—are overstoichiometric in carbon. As EDS quantification of light

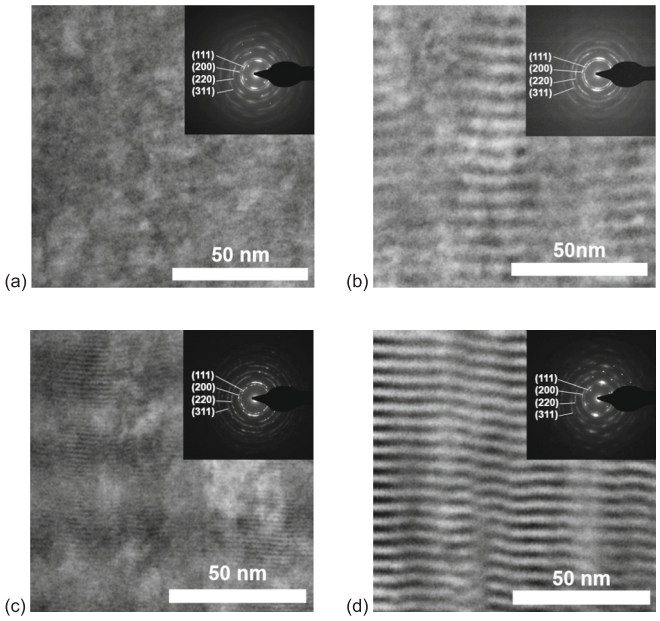

Fig. 2. STEM cross sections of (a) TaC/HfC with Λ_{nom} = 2 nm, (b) TaC/HfC with Λ_{nom} = 6 nm, (c) TiC/TaC with Λ_{nom} = 2 nm, (d) TiC/TaC with Λ_{nom} = 6 nm coatings. The insets are respective SAED patterns taken from the region close to the interface to the Si(100) substrate.

and heavy elements based on theoretically estimated k-factors is complex and strongly depends on the chosen acceleration voltage [28], we also selected a few samples for more accurate elastic recoil detection analysis (ERDA). These (not shown here) also exhibit a slight over-stoichiometric carbon to metal ratio (C/Me) for HfC, TaC, TiC, and TaC/HfC (Λ_{nom} = 6 nm) superlattice, which agrees well with the EDS measurements. Carbon to metal ratios above one for coatings with a solely NaCl-type crystal structure may stem from a higher vacancy content at the metal sublattice or excess carbon at grain and column boundaries. Especially for non-reactive deposition—as used here—the latter is not likely. When concentrating on the metal ratio, the TaC/HfC coatings exhibit a close to 1/1 ratio, see Fig. 3a. In agreement with STEM investigations, this proves their balanced layer thickness ratio. The TiC/TaC coatings exhibit a slightly higher Ta content, indicating that the TaC layers are slightly thicker than the TiC layers.

3.4. Mechanical properties

Fig. 4a shows that the TaC/HfC coatings do not exhibit a superlattice effect (for the investigated bilayer periods) in hardness (H), as all values are essentially between those of the monolithically grown constituents TaC (H = 33.3 ± 1.9 GPa) and HfC (H = 37.4 ± 3.2 GPa). Out of the TaC/HfC coatings the one with Λ_{nom} = 2 nm is the hardest with 36.0 ± 1.6 GPa, but TEM investigations (Fig. 2a) proved this to rather be a solid solution than a layered material. The indentation moduli E of the TaC/HfC coatings lie between those of the constituting layers TaC (E = 329 ± 15 GPa) and HfC (E = 351 ± 20GPa) for larger bilayer periods, whereas that with Λ_{nom} = 2 nm provides the highest value with 377 ± 22 GPa, which is even above that of HfC. Based purely on solid solution effects, the E modulus should follow the rule of mixture whereas H should be higher. Thus, the solid solution strengthening effect seems to be not pronounced for the TaC/HfC coatings with Λ_{nom} = 2 nm. Still the combination of H = 36.0 ± 1.6 GPa with E = 377 ± 22 GPa is excellent, and Ta-Hf-C materials are often named as those with the highest melting points [29].

The TiC/TaC superlattice coatings show a different behavior, with a pronounced hardness maximum (44.1 ± 3.4 GPa) for Λ_{nom} = 2 nm, and also the TiC/TaC coatings with larger bilayer periods of Λ_{nom} = 6 and 10 nm still outperform with ~39 GPa the hardest of their constituents (TiC, H = 37.6 ± 3.1 GPa). Their indentation moduli are between those of TiC (E = 291 ± 13 GPa) and TaC (E = 330 ± 15 GPa) essentially without a dependence on Λ.

When calculating the H/E ratio, which is often-used for assessing the energy dissipation ability of ceramics [30], the TiC/TaC coatings would show slightly higher values than the TaC/HfC ones. For the TiC/TaC coatings, the H/E ratio peaks (with 0.14) for the same superlattice period (2 nm) as the hardness. Thus, in agreement with earlier studies on transition metal nitride superlattices [10], also for the TiC/TaC coatings such a combined superlattice effect on hardness and toughness is present.

Figs. 5a, b, c and d show cube corner imprints of the monolithically grown carbide (TiC) and the TiC/TaC and TaC/HfC superlattice coatings (with Λ_{nom} = 2 nm and Λ_{nom} = 10 nm), respectively. The TiC coating exhibits the shortest cracks among the three monolithically grown carbides. Severe delamination occurs during indentation for TaC and HfC monolithic films as well as the TaC/HfC Λ_{nom} = 2 nm "superlattice". For the Λ_{nom} = 6 nm TaC/HfC superlattice, the Λ_{nom} = 2 nm and Λ_{nom} = 6 nm TiC/TaC superlattices, delamination, lateral/ penny cracks and buckling of different degrees occur. The hardest material, the TiC/TaC Λ_{nom} = 2 nm, very similarly to the TaC/HfC Λ_{nom} = 6 nm film, exhibits low fracture resistance featuring delamination and lateral cracking, see Fig. 5c. The TiC/TaC Λ_{nom} = 6 nm coating exhibits a fracture behavior similarly to TaC. Still, all TaC/HfC superlattices and the TiC/TaC Λ_{nom} = 10 nm outperform their individual constituents during this qualitative fracture behavior experiment, in terms of both cracking and delamination behavior. Out of the superlattices those with Λ_{nom} = 10 nm behaved best. The TiC/TaC superlattice, Fig. 5c, even shows no radial crack formation. [31]

4. Discussion

The TaC/HfC coatings exhibit a clear superlattice structure for Λ_{nom} = 6 and 10 nm during XRD as well as TEM investigations. In contrast, the Λ_{nom} = 2 nm coating actually shows more solid solution-like features during these studies. The lattice parameter difference between TaC and HfC is 0.019 nm (δ = 4.2%) and their indentation moduli differ by 21 GPa (the DFT obtained shear moduli by 23 GPa, Table 1). Although experimentally obtained lattice parameter misfits are slightly smaller than the calculated ones (Table 1), the individual layers experience lateral cracks during cube corner indentations (see Fig. 5c). This might contribute to the missing superlattice effect for the hardness; all TaC/HfC coatings studied show a hardness between those of TaC (H = 33.3 ± 1.9 GPa) and HfC (H = 37.4 ± 3.2 GPa).

The TiC/TaC constituents allow forming of superlattices also for the smallest bilayer period studied, Λ_{nom} = 2 nm. Although this coating shows no pronounced superlattice reflexes during XRD (Fig. 1), TEM

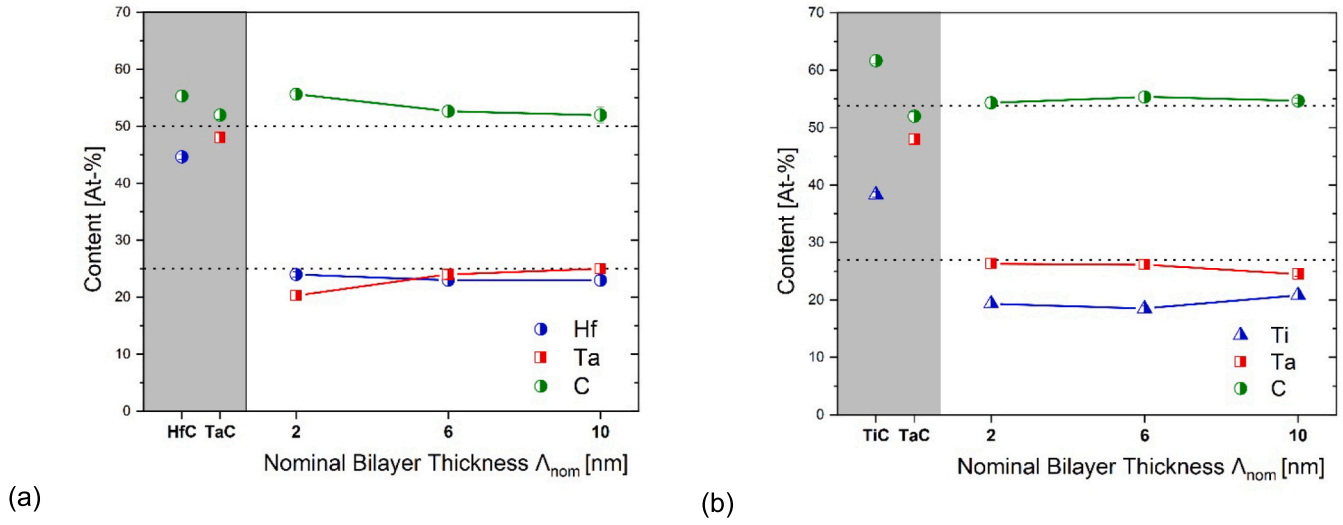

Fig. 3. EDS obtained chemical composition of (a) TaC/HfC and (b) TiC/TaC coatings and their respective monolithically grown constituents.

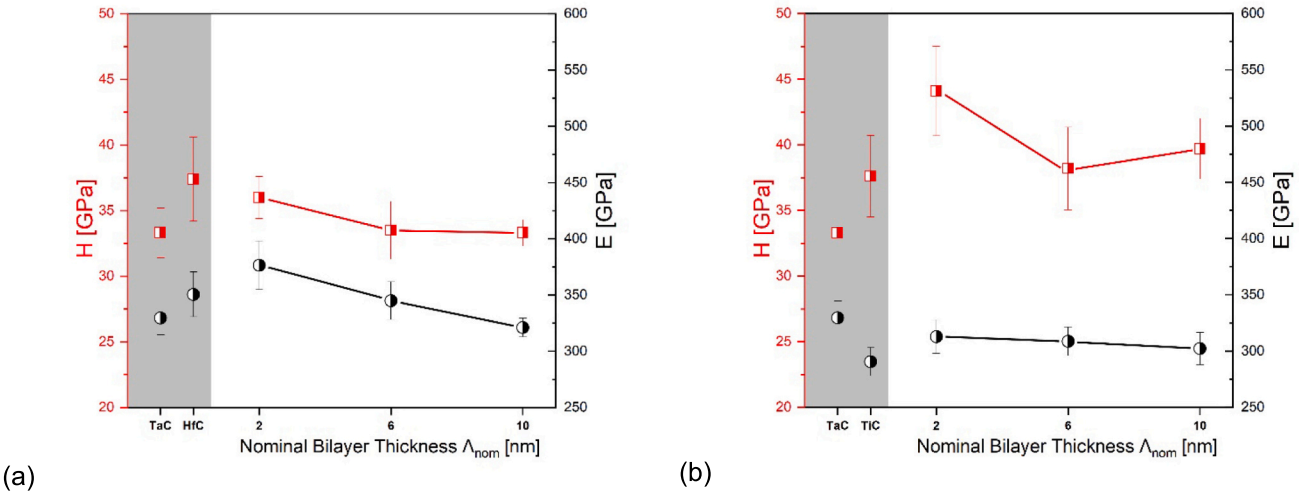

Fig. 4. Hardness (*H*, red squared symbols) and indentation modulus (*E*, black round symbols) for the monolithically prepared coatings and their superlattices. (a) TaC/HfC and (b) TiC/TaC system. (For interpretation of the references to colour in this figure legend, the reader is referred to the web version of this article.)

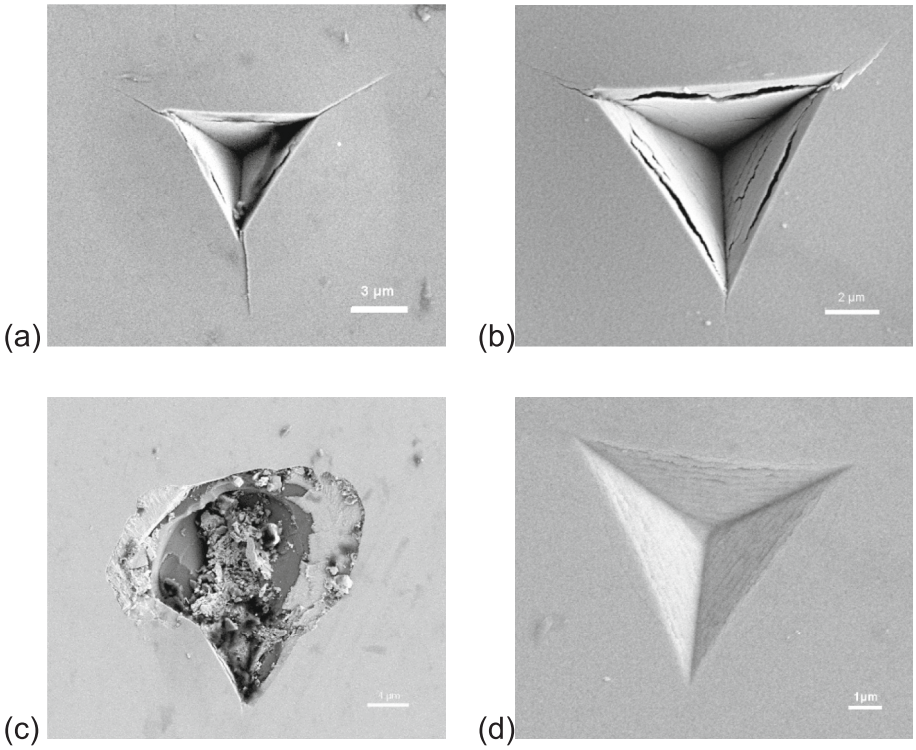

Fig. 5. Cube corner imprints into (a) TiC, (b) TaC/HfC with $\Lambda_{nom} = 10$ nm, (c) TiC/TaC with $\Lambda_{nom} = 2$ nm and (d) TiC/TaC with $\Lambda_{nom} = 10$ nm coatings obtained with a load of 450 mN. Magnifications differ between the images to capture the indents entirely.

studies clearly prove their layered arrangement (Fig. 2) with an experimentally obtained bilayer period of 1.66 nm. The lattice parameter mismatch between TiC and TaC is 0.011 nm ($\delta = 2.4\%$) and their indentation moduli differ by 39 GPa (the DFT obtained shear moduli by 19 GPa, Table 1). Hence, compared with TaC/HfC, the lattice parameter mismatch is smaller but the indentation modulus mismatch is more significant. Contrary to the TaC/HfC coatings, only tiny lateral cracks are present in the imprints of the cube corner indentation experiments (with the same maximum load of 450 mN as used for the TaC/HfC superlattice, which exhibits pronounced lateral cracks, compare Fig. 5b). Furthermore, the TiC/TaC superlattices exhibit a well-developed hardness peak of 44.1 ± 3.4 GPa at $\Lambda_{nom} = 2$ nm, which is a clear hardness improvement (+ 6.5 GPa) compared to the TiC coating (being the harder of the two constituting compounds). Preliminary qualitative fracture behavior investigations—by cube corner indentation experiments—also suggest an improvement, especially for the superlattice coatings with $\Lambda_{nom} = 10$ nm. Further, fracture toughness seems to improve with higher bilayer periods for all superlattices.

5. Conclusions

Non-reactive unbalanced magnetron sputtering—from the respective transition metal carbide targets—allows the growth of phase-pure face centred cubic structured TaC, HfC, and TiC coatings. Combining these

materials, we were able to develop TaC/HfC superlattices with $\Lambda_{nom} = 6$ and 10 nm and TiC/TaC superlattices with $\Lambda_{nom} = 2$, 6, and 10 nm. Detailed cross-sectional TEM studies proved their layered arrangement with symmetric bilayers and a more solid solution-like structure for the TaC/HfC coating with $\Lambda_{nom} = 2$ nm. The even distribution of the bilayer period among the constituting layers fits very well with the EDS results, showing an almost 1/1 ratio of the respective transition metals.

Contrary to the TaC/HfC superlattices, which exhibit no superlattice effect in hardness, the TiC/TaC superlattices exhibit a peak in hardness with 44.1 ± 3.4 GPa for $\Lambda_{nom} = 2$ nm. This value is, with an increase in hardness of 6.5 GPa, clearly above that of the hardest constituting layer, TiC, having 37.6 ± 3.1 GPa. Qualitative cube corner indentation experiments furthermore suggest a higher fracture resistance for the TiC/TaC superlattices than obtained for the TaC/HfC superlattices as well as TaC, HfC, and to some degree even TiC coatings. The TiC/TaC superlattice with $\Lambda_{nom} = 10$ nm exhibits the tiniest lateral cracks during cube corner indentation experiments among all coatings studied.

Based on our results we can conclude that the combination of TiC and TaC is superior to that of HfC and TaC in terms of hardness improvement as well as fracture resistance. Based on DFT data, the shear moduli difference is rather similar between TaC and HfC (23 GPa) as well as between TiC and TaC (19 GPa). But their lattice parameter mismatch δ is 4.2% for the TaC/HfC combination whereas only 2.4% for the TiC/TaC combination.

Funding

This research did not receive any specific grant from funding agencies in the public, commercial, or non-profit sectors.

CRediT authorship contribution statement

Barbara Schmid: Writing – original draft, Data curation, Investigation, Visualization. **Nikola Koutná:** Formal analysis, Writing – review & editing. **Rainer Hahn:** Writing – review & editing. **Tomasz Wojcik:** Investigation. **Peter Polcik:** Resources. **Paul Heinz Mayrhofer:** Conceptualization, Resources, Writing – review & editing, Funding acquisition.

Declaration of Competing Interest

The authors declare that they have no known competing financial interests or personal relationships that could have appeared to influence the work reported in this paper.

Data availability

Data will be made available on request.

Acknowledgements

We thank the Vienna Scientific Cluster for the attribution of computation time and Plansee Composite materials for providing resources. The authors acknowledge the use of the facilities of USTEM and XRC at TU Wien, as well as TU Wien Bibliothek for financial support through its Open Access Funding Program.

References

[1] P.H. Mayrhofer, A. Kirnbauer, P. Ertelthaler, C.M. Koller, High-entropy ceramic thin films; a case study on transition metal diborides, Scr. Mater. 149 (2018) 93–97, https://doi.org/10.1016/j.scriptamat.2018.02.008.
[2] D.G. Sangiovanni, L. Hultman, I. Petrov, J.E. Greene, Elastic properties and plastic deformation of TiC- and VC-based pseudobinary alloys, Acta Mater. 144 (2018) 376–385, https://doi.org/10.1016/j.actamat.2017.10.047.
[3] H. Liang, et al., Insights into the bond behavior and mechanical properties of hafnium carbide under high pressure and high temperature, Inorg. Chem. 60 (2) (2021) 515–524, https://doi.org/10.1021/acs.inorgchem.0c02800.
[4] Q.Q. Bai, Y. Bai, 12 fatigue and fracture, in: Subsea Pipeline Design, Analysis, and Installation, 2014, pp. 283–318.
[5] U. Helmersson, S. Todorova, S.A. Barnett, J. Sundgren, Growth of single-crystal TiN/VN slrained-layer superlattices with extremely high mechanical hardness 481 (1987) (2003) 1–5.
[6] X. Chu, S.A. Barnett, Model of superlattice yield stress and hardness enhancements, J. Appl. Phys. 77 (9) (1995) 4403–4411, https://doi.org/10.1063/1.359467.
[7] P.B. Mirkarimi, L. Hultman, S.A. Barnett, Enhanced hardness in lattice-matched single-crystal TiN/V0.6Nb0.4N superlattices 2654 (June) (1998) 1–4.
[8] J.W. Gahn, Hardening by spinodal decomposition, Acta Metall. 11 (12) (1963) 1275–1282, https://doi.org/10.1016/0001-6160(63)90022-1.
[9] J.S. Koehler, Attempt to design a strong solid, Phys. Rev. B 2 (2) (1970) 547–551, https://doi.org/10.1103/PhysRevB.2.547.
[10] R. Hahn, M. Bartosik, R. Soler, C. Kirchlechner, G. Dehm, P.H. Mayrhofer, Superlattice effect for enhanced fracture toughness of hard coatings, Scr. Mater. 124 (2016) 67–70, https://doi.org/10.1016/j.scriptamat.2016.06.030.
[11] A. Wagner, D. Holec, P.H. Mayrhofer, M. Bartosik, Enhanced fracture toughness in ceramic superlattice thin films: on the role of coherency stresses and misfit dislocations, Mater. Des. 202 (2021), 109517, https://doi.org/10.1016/j.matdes.2021.109517.
[12] J. Buchinger, et al., Toughness enhancement in TiN/WN superlattice thin films, Acta Mater. 172 (2019) 18–29, https://doi.org/10.1016/j.actamat.2019.04.028.
[13] R. Hahn, et al., Mechanistic study of superlattice-enabled high toughness and hardness in MoN/TaN coatings, Commun. Mater. 1 (1) (2020), https://doi.org/10.1038/s43246-020-00064-4.
[14] N. Koutná, et al., Point-defect engineering of MoN/TaN superlattice films: a first-principles and experimental study, Mater. Des. 186 (2020), 108211, https://doi.org/10.1016/j.matdes.2019.108211.
[15] J. Buchinger, et al., Fracture toughness trends of modulus-matched TiN/(Cr,Al)N thin film superlattices, Acta Mater. 202 (January) (2021) 376–386, https://doi.org/10.1016/j.actamat.2020.10.068.
[16] Zecui Gao, Julian Buchinger, Nikola Koutná, Tomasz Wojcik, Rainer Hahn, H. Mayrhofer Paul, Ab Initio Supported Development of TiN/MoN Superlattice Thin Films with Improved Hardness and Toughness, 2020, pp. 1–35. Available at SSRN: https://ssrn.com/ab.
[17] C. Mitterer, et al., Industrial applications of PACVD hard coatings, Surf. Coat. Technol. 163-164 (2003) 716–722, https://doi.org/10.1016/S0257-8972(02)00685-0.
[18] G. Kresse, J. Furthmüller, Efficient iterative schemes for ab initio total-energy calculations using a plane-wave basis set, Phys. Rev. B 54 (1996) 11169–11186, https://doi.org/10.1103/PhysRevB.54.11169.
[19] G. Kresse, D. Joubert, From ultrasoft pseudopotentials to the projector augmented-wave method, Phys. Rev. B - Condens. Matter Mater. Phys. 59 (3) (1999) 1758–1775, https://doi.org/10.1103/PhysRevB.59.1758.
[20] N. Koutná, A. Brenner, D. Holec, P.H. Mayrhofer, High-throughput first-principles search for ceramic superlattices with improved ductility and fracture resistance, Acta Mater 206 (March) (2021) 1–17, https://doi.org/10.1016/j.actamat.2020.116615.
[21] S. Logothetidis, N. Kalfagiannis, K. Sarakinos, P. Patsalas, Investigation of bilayer period and individual layer thickness of CrN / TiN superlattices by ellipsometry and X-ray techniques, Surf. Coatings Technol. 200 (2006) 6176–6180, https://doi.org/10.1016/j.surfcoat.2005.11.022.
[22] A.C. Fischer-Cripps, Critical review of analysis and interpretation of nanoindentation test data, Surf. Coatings Technol. 200 (14–15) (2006) 4153–4165, https://doi.org/10.1016/j.surfcoat.2005.03.018.
[23] E. Tarrés, G. Ramírez, Y. Gaillard, E. Jiménez-Piqué, L. Llanes, Contact fatigue behavior of PVD-coated hardmetals, Int. J. Refract. Met. Hard Mater. 27 (2) (2009) 323–331, https://doi.org/10.1016/j.ijrmhm.2008.05.003.
[24] P. Sarker, et al., High-entropy high-hardness metal carbides discovered by entropy descriptors, Nat. Commun. 9 (1) (2018) 1–10, https://doi.org/10.1038/s41467-018-07160-7.
[25] H. Lasfargues, et al., Non-reactively sputtered ultra-high temperature Hf-C and Ta-C coatings, Surf. Coatings Technol. 309 (2017) 436–444, https://doi.org/10.1016/j.surfcoat.2016.11.073.
[26] K. Aigner, W. Lengauer, D. Rafaja, P. Ettmayer, Lattice parameters and thermal expansion of Ti(CxN1-x), Zr(CxN1-x), Hf(CxN1-x) and TiN1-x from 298 to 1473 K as investigated by high-temperature X-ray diffraction, J. Alloys Compd. 215 (1–2) (1994) 121–126, https://doi.org/10.1016/0925-8388(94)90828-1.
[27] R.W.G. Wyckoff, The Structure of Crystals, 2nd ed., The Chemical Catalogue Company, New York, 1931.
[28] T. Transactions, C. Techniczne, An analysis of the elemental composition of micro-samples using EDS technique, Tech. Trans. 2014 (2014) 133–148, https://doi.org/10.4467/2353737XCT.14.283.3371.
[29] Q.J. Hong, A. Van De Walle, Prediction of the material with highest known melting point from ab initio molecular dynamics calculations, Phys. Rev. B - Condens. Matter Mater. Phys. 92 (2) (2015) 1–6, https://doi.org/10.1103/PhysRevB.92.020104.
[30] Y. Bao, D. Wan, Y. Qiu, Estimating energy dissipation of ceramics via H-E ratio, Key Eng. Mater. 434–435 (2010) 205–208, https://doi.org/10.4028/www.scientific.net/KEM.434-435.205.
[31] J. Chen, Indentation-based methods to assess fracture toughness for thin coatings, J. Phys. D. Appl. Phys. 45 (20) (2012), 203001, https://doi.org/10.1088/0022-3727/45/20/203001.

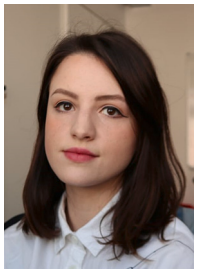

Barbara Schmid is a PhD candidate in the research group of Paul Heinz Mayrhofer at TU Wien, where she specializes in sputter deposited transition metal carbide and nitride multilayer systems. Her aim is to investigate chemical, mechanical and electrical properties of ceramic materials and improve those characteristics. She received her master's degree from TU Wien in technical chemistry in 2020.

Nikola Koutná is a computational materials scientist developing design guidelines for thin films with targeted architecture and mechanical properties. She received her PhD from TU Wien, Austria, in 2021 and is currently a postdoc at TU Wien (Hertha Firnberg grant) and the Linköping University, Sweden. Her main focus is ab initio and (ab initio) molecular dynamics calculations, with the aim to develop atomic-level understanding of strength and plasticity mechanisms in layered ceramic-based systems.

Rainer Hahn holds an MSc degree inMaterials Science from theMontanuniversitaet Leoben, Austria(2016) and received his Ph.D. in 2019 from TU Wien (Austria). Currently, he is pursuing his academic career at TU Wien in the Christian Doppler Laboratory for Surface Engineering of high-performance Components. His research focuses on micromechanical experiments, especially fracture toughness measurements, on hard and functional PVD-deposited coatings applicable in the aerospace and energy conversion industry.

Tomasz Wojcik is an electron microscopy specialist, working in this field for over 10 years. His research mainly includes phase and microstructure characterization in metals, hard coatings, and semiconductors, applying techniques like TEM, EDS, EELS, SAED, SEM, EBSD, and TKD. Currently, he is employed as senior scientist at the Institute of Materials Science and Technology, TU Wien, Austria.

Peter Polcik is a Product Development Manager at Plansee Composite Materials GmbH, Lechbruck, Germany. He received a PhD in Materials Science from Friedrich-Alexander University Erlangen-Nürnberg, Germany, in 1998. After which he started to work for Plansee in Reutte, Austria, as a head of R&D in the field of target and cathode materials for hard coating applications. Since 2006 he is responsible for Development, Marketing and Production in this business field at Plansee CM GmbH in Lechbruck, Germany. He established a strong network for advanced hard coatings between industry, research institutes and Plansee; being a target supplier and R&D partner.

Paul Heinz Mayrhofer is University Professor of Materials Science and chairs this division at TU Wien. He habilitated in 2005 and received a Dr. in 2001 in Materials Science at the University of Leoben. He spent his post-doc and Erwin-Schrödinger-Fellowship at the University of Illinois at Urbana-Champaign, RTWH Aachen, and Linkoping University. His research activities focus on the development and characterization of vapor phase deposited nanostructured materials by a combination of computational and experimental material science. He is a member of the Austrian Academy of Sciences and Fellow of the American Vacuum Society.